Ablation of specific expression domains reveals discrete functions of ectoderm- and endoderm-derived FGF8 during cardiovascular and pharyngeal development

Timothy L. Macatee[1], Benjamin P. Hammond[1,2], Benjamin R. Arenkiel[3], Lily Francis[4], Deborah U. Frank[2,5] and Anne M. Moon[1,2,3,5,6,*]

[1]Program in Human Molecular Biology and Genetics, University of Utah School of Medicine, Salt Lake City, UT 84112, USA
[2]Childrens Health Research Center, University of Utah School of Medicine, Salt Lake City, UT 84112, USA
[3]Program in Molecular Biology, University of Utah School of Medicine, Salt Lake City, UT 84112, USA
[4]Program in Neuroscience, University of Utah School of Medicine, Salt Lake City, UT 84112, USA
[5]Department of Pediatrics, University of Utah School of Medicine, Salt Lake City, UT 84112, USA
[6]Department of Neurobiology and Anatomy, University of Utah School of Medicine, Salt Lake City, UT 84112, USA
*Author for correspondence (e-mail: anne.moon@genetics.utah.edu)

Development 130, 6361-6374
Published by The Company of Biologists 2003
doi:10.1242/dev.00850

Accepted 4 September 2003

Summary

Fibroblast growth factor 8 (*Fgf8*) is expressed in many domains of the developing embryo. Globally decreased FGF8 signaling during murine embryogenesis results in a hypomorphic phenotype with a constellation of heart, outflow tract, great vessel and pharyngeal gland defects that phenocopies human deletion 22q11 syndromes, such as DiGeorge. We postulate that these *Fgf8* hypomorphic phenotypes result from disruption of local FGF8 signaling from pharyngeal arch epithelia to mesenchymal cells populating and migrating through the third and fourth pharyngeal arches.

To test our hypothesis, and to determine whether the pharyngeal ectoderm and endoderm *Fgf8* expression domains have discrete functional roles, we performed conditional mutagenesis of *Fgf8* using novel Cre-recombinase drivers to achieve domain-specific ablation of *Fgf8* gene function in the pharyngeal arch ectoderm and endoderm.

Remarkably, ablating FGF8 protein in the pharyngeal arch ectoderm causes failure of formation of the fourth pharyngeal arch artery that results in aortic arch and subclavian artery anomalies in 95% of mutants; these defects recapitulate the spectrum and frequency of vascular defects reported in *Fgf8* hypomorphs. Surprisingly, no cardiac, outflow tract or glandular defects were found in ectodermal-domain mutants, indicating that ectodermally derived FGF8 has essential roles during pharyngeal arch vascular development distinct from those in cardiac, outflow tract and pharyngeal gland morphogenesis. By contrast, ablation of FGF8 in the third and fourth pharyngeal endoderm and ectoderm caused glandular defects and bicuspid aortic valve, which indicates that the FGF8 endodermal domain has discrete roles in pharyngeal and valvar development. These results support our hypotheses that local FGF8 signaling from the pharyngeal epithelia is required for pharyngeal vascular and glandular development, and that the pharyngeal ectodermal and endodermal domains of FGF8 have separate functions.

Key words: Cardiovascular development, Pharyngeal arch, FGF8, Endoderm, Heart field, Pharyngeal arch artery, Congenital heart disease, Vasculogenesis, Aortic arch, Outflow tract, Coronary artery, Thymus, Parathyroid, 22q11 deletion syndrome, DiGeorge Syndrome

Introduction

The pharyngeal arches (PAs) consist of mesenchyme encased in ectoderm and endoderm. PA mesenchyme is derived from paraxial mesoderm and neural crest (NC, ectomesenchyme). Mesoderm-derived mesenchyme contributes muscular and endothelial precursors to the PAs. Some of the ectomesenchyme gives rise to skeletal structures, and to pericytes and smooth muscle cells of the pharyngeal arch arteries (PAAs), while a different population traverses the PAs en route to forming parts of the outflow tract (OFT) and heart (Jiang et al., 2000; Li et al., 2000). A PAA forms within each arch, connecting the heart to the bilateral dorsal aortae; this initially symmetric vascular array is extensively remodeled during development. This morphogenetic process is coordinately regulated by a number of signaling pathways that, if perturbed, can result in aberrant formation and/or remodeling of the PAAs and lethal congenital cardiovascular malformations.

Fgf8 encodes a crucial member of the FGF family (MacArthur et al., 1995). Secreted FGF8 protein provides survival, mitogenic, anti/pro-differentiation and patterning signals to adjacent tissues, and may also have autocrine activity. Complete ablation of *Fgf8* function in mice results in early embryonic lethality at approximately embryonic day (E)

8.5 (Meyers et al., 1998; Moon and Capecchi, 2000; Sun et al., 1999). We and others have thus employed hypomorphic and conditional alleles to study its role in limb, face, brain, cardiovascular and pharyngeal development (Abu-Issa et al., 2002; Frank et al., 2002; Garel et al., 2003; Meyers et al., 1998; Meyers and Martin, 1999; Moon et al., 2000; Moon and Capecchi, 2000; Storm et al., 2003; Sun et al., 2000; Trumpp et al., 1999).

Fgf8 mutations in several species demonstrate its role(s) in early cardiovascular and PA development. Zebrafish *acerebellar Fgf8* mutants have abnormal cardiogenesis, ventricular hypoplasia and circulatory failure (Reifers et al., 2000). Removal of *Fgf8*-expressing endoderm adjacent to precardiac mesoderm in chicks alters expression of cardiac markers such as *Nkx2.5* (Alsan and Schultheiss, 2002).

In the mouse, *Fgf8* is expressed in several temporospatial domains that are potentially relevant to cardiovascular and pharyngeal development. These include the precardiac mesoderm (Crossley and Martin, 1995), the early foregut endoderm and later, in restricted regions of PA endoderm and ectoderm. Murine *Fgf8* hypomorphic mutants (mice with globally decreased FGF8 signaling throughout embryogenesis) have severe cardiovascular and pharyngeal defects, including altered cardiac outflow tract (OFT) alignment and septation, disrupted pharyngeal vascular development, and abnormal formation of the thymus and parathyroids (Abu-Issa et al., 2002; Frank et al., 2002). These *Fgf8* hypomorphs phenocopy human syndromes associated with deletion of chromosome 22q11 (del22q11) such as DiGeorge syndrome (Epstein, 2001; Frank et al., 2002; Lindsay, 2001; Scambler, 2000). Furthermore, *Fgf8* genetically interacts with *Tbx1* (Vitelli et al., 2002), a gene located in the human del22q11 region known to play a crucial role in generating human del22q11 phenotypes (Jerome and Papaioannou, 2001; Lindsay et al., 2001; Merscher et al., 2001). Thus, delineating the function of specific FGF8 signaling domains and downstream pathways will provide insight into how their dysfunction results in the spectrum of birth defects seen in human del22q11syndromes.

Although the *Fgf8* hypomorphic model provides enormous insight into the importance of FGF8 signaling during cardiovascular and pharyngeal development, it does not allow us to test the role of local (pharyngeally produced) FGF8 in development of the pharynx or cardiovascular system, or to dissect the respective role(s) of different *Fgf8* expression domains that are relevant to these morphogenetic processes. Furthermore, analyses of the molecular and cellular pathways that are disrupted by loss of a specific *Fgf8* expression domain cannot be assessed with this system.

We have postulated that the *Fgf8* hypomorph cardiovascular and pharyngeal phenotypes result from disrupted local FGF8 signaling from the epithelia of PAs 3-6 to mesenchymal cells populating and migrating through these arches, including cardiac neural crest en route to the OFT (Frank et al., 2002). To test this hypothesis, and to determine whether FGF8 signals emanating from the pharyngeal ectoderm and endoderm perform discrete functions, we generated a unique series of *Fgf8* conditional alleles and Cre recombinase-expressing drivers designed to ablate FGF8 in different pharyngeal epithelial domains.

Materials and methods

Mutant mouse strains

The strategy for homologous recombination in ES cells used to target *Fgf8*, and the other loci noted below, was as previously described (Moon et al., 2000).

Conditional alleles of *Fgf8*

The conditional alleles employed in this study are shown schematically in Fig. 1. Insertion of the GFP reporter gene into the 3′ untranslated region of *Fgf8* was performed as previously described for the $Fgf8^{APN}$ hypomorphic, conditional reporter allele (Frank et al., 2002; Moon and Capecchi, 2000). The $Fgf8^{null}$ allele, resulting from removal of exon 5, has also been reported (Moon and Capecchi, 2000). Mutant embryos are in a 75% C57Bl6, 25% SV129 background.

AP2α-IRESCre driver

An ectodermal domain-specific ‘Cre driver’ was generated by targeting an IRESCre cassette into the 3′ untranslated region of the *AP2α* locus (Fig. 2A). This cassette contains an Internal Ribosomal Entry Site, IRES (Jackson et al., 1990; Jang and Wimmer, 1990), upstream of the Cre recombinase gene (Sauer and Henderson, 1988) and an frt-flanked neomycin phosphotransferase gene (Fig. 2A). Placing the IRESCre cassette between the stop codon and the endogenous poly-adenylation signal allows regulation of Cre expression by the *AP2α* locus with intact *AP2α* gene function.

Hoxa3-IRESCre driver

To ablate FGF8 in both the endoderm and ectoderm of PAs 3-6, we targeted the IRESCre cassette into the *hoxa3* locus in a genomic *Apa*I site located 3′ of the stop codon (Fig. 3A).

Alkaline phosphatase staining

Alkaline phosphatase staining was performed as previously described (Moon et al., 2000).

TUNEL analysis and immunohistochemistry

Somite/stage-matched embryos were fixed and whole mount terminal UTP nick end labeled (TUNEL) assays performed as described previously (Frank et al., 2002; Stadler et al., 2001).

Whole-mount green fluorescent protein (GFP) detection was performed on whole embryos using a rabbit anti-GFP and FITC-conjugated anti-rabbit IgG secondary antibodies (1:1000 and 1:500, respectively, both from Molecular Probes).

For cryosectioned specimens, embryos were protected in sucrose and gelatin-embedded. Cryosections (12 μm) were cut transversely, parallel to the third PAA. The Ap2α transcription factor, which is expressed in neural crest and ectoderm, was detected with a mouse monoclonal anti-AP2α-antibody (1:25, 3B5, Developmental Studies Hybridoma Bank) and a FITC-conjugated anti-mouse IgG secondary (1:500, Molecular Probes). Simultaneous TUNEL was performed by adding the TMR Red in situ cell death detection reagents (Roche) to secondary antibody incubation. Sections were preserved in Fluoromount-G (Southern Biotechnology Associates) and analyzed by confocal microscopy. FITC and Texas red fluorescence were recorded using a BioRad MRC 1024 laser-scanning confocal imaging system fitted to a Leitz Aristoplan microscope. A digital Kalman averaging filter was used to reduce background fluorescence.

Results

Elements of the conditional mutagenesis system

Conditional alleles of *Fgf8*

Since *Fgf8* null homozygotes die at approximately E8.5 due to defects in gastrulation (Meyers et al., 1998; Moon and

Capecchi, 2000; Sun et al., 1999), conditional mutagenesis is required to study the different roles of this protein during murine development.

We previously described a conditional reporter allele, *Fgf8*^{APN}, that is hypomorphic due to the presence of a neo^{r} gene in the 3′ untranslated region of the *Fgf8* locus (Frank et al., 2002; Moon and Capecchi, 2000) (Fig. 1A). Mice bearing this allele and a null allele of *Fgf8* are hypomorphs (genotype *Fgf8*$^{APN/null}$) and die at birth with the aforementioned complex phenotype (Frank et al., 2002).

For the current study, we modified the *Fgf8*^{APN} allele by removing the frt-flanked neo^{r} gene with flp-mediated recombination in the germline of founder animals (Dymecki, 1996) (Fig. 1B). The resulting *Fgf8*^{AP} allele is not hypomorphic. *Fgf8*$^{AP/null}$ compound heterozygotes survive and are phenotypically normal (see Fig. 4A). The *Fgf8*^{AP} allele was also designed as a conditional reporter allele: exon 5 is flanked with loxP sites and coding sequences for human alkaline phosphatase (AP) are positioned in the 3′ untranslated region of *Fgf8*. Cre-mediated recombination of this allele removes exon 5 and allows expression of the AP reporter gene under control of the *Fgf8* promoter.

We also generated a second nonhypomorphic conditional reporter allele, *Fgf8*^{GFP}, using the strategy described for the *Fgf8*^{AP} allele. *Fgf8*^{GFP} functions identically to *Fgf8*^{AP} except that green fluorescent protein (GFP) is produced upon Cre-mediated recombination of the allele.

Expression of either reporter gene depends on: (1) Cre-mediated recombination of *Fgf8*^{AP} or *Fgf8*^{GFP} to generate the *Fgf8*^{APR} and *Fgf8*^{GFPR} null reporter alleles (Fig. 1C) and (2) activity of the *Fgf8* locus. These reporters permit precise determination of the temporospatial inactivation of *Fgf8* in cells in which it is expressed (Moon et al., 2000; Moon and Capecchi, 2000).

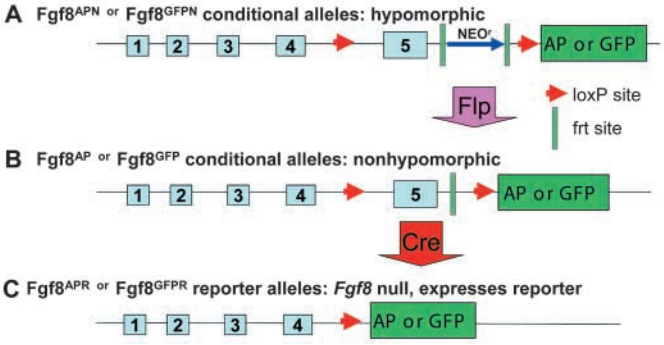

Fig. 1. Nonhypomorphic, conditional reporter alleles of *Fgf8* used for domain-specific ablation experiments. (A) Different cassettes were inserted into the 3′ UTR of *Fgf8* to generate the *Fgf8*^{APN} and *Fgf8*^{GFPN} alleles. An in-frame splice acceptor and the alkaline phosphatase (AP) or green fluorescent protein (GFP) reporter genes (green boxes) were positioned downstream of the 3′ loxP site (red arrowheads) and an frt-flanked neo^{r} gene (green bars flanking labeled arrow) in a *Spe*I site located in the 3′UTR of *Fgf8*. These alleles are hypomorphic because the presence of neo^{r}. Flp-mediated recombination (purple arrow) of frt sites (green bars) deletes the neo^{r} gene and generates nonhypomorphic conditional reporter alleles, *Fgf8*^{AP} and *Fgf8*^{GFP}. *Fgf8*^{AP} and *Fgf8*^{GFP} alleles are inactivated with respect to production of functional *Fgf8* message when Cre (large red arrow) recombines the loxP sites (red arrowheads) to delete exon 5 (Moon and Capecchi, 2000). Recombination results in expression of the AP or GFP reporter gene under control of *Fgf8* regulatory sequences (*Fgf8*^{APR}, *Fgf8*^{GFPR}), allowing detection of functionally relevant recombination of *Fgf8* (i.e. inactivation of *Fgf8* in cells in which it is expressed).

Domain-specific Cre-recombinase drivers for conditional ablation of FGF8 in the pharyngeal epithelia

Deletion of exon 5 from the of *Fgf8*^{AP} or *Fgf8*^{GFP} conditional alleles depends on expression and activity of Cre-recombinase. We obtained spatial and temporal control over Cre by inserting an IRES followed by Cre-encoding sequences into the 3′ untranslated region of two genes that are expressed in pharyngeal domains of interest, the *Ap2α* and *hoxa3* loci (see Materials and methods; Fig. 2A, Fig. 3A). As described in detail below, to determine whether expression of these targeted Cre drivers recapitulated the pattern of the endogenous loci, we examined the expression of the global Cre reporter gene, *Rosa26*^{lacZ} (Soriano, 1999). Cre-mediated recombination of the *Rosa26*^{lacZ} allele results in β-galactosidase production from the recombined, constituitively expressed *Rosa26* locus. Furthermore, we determined the domains of functionally relevant recombination of *Fgf8* obtained with these Cre drivers by characterizing expression of recombined *Fgf8* conditional reporter alleles in the developing PAs.

AP2α-IRESCre ablates FGF8 signaling from the PA ectoderm

We ablated *Fgf8* gene function in its PA ectodermal expression domains from the time of PA formation with the targeted *AP2α-IRESCre* driver (Fig. 2A,B). The *AP2α* gene is expressed in many regions of the mouse embryo (Mitchell et al., 1991), including pharyngeal NC and ectoderm (Brewer et al., 2002). Lineage analyses of the *AP2α-IRESCre* driver in the PAs were performed by crossing this allele into mice bearing the *Rosa26*^{lacZ} allele (genotype AP2*α*$^{IRESCre/+}$; *Rosa26*$^{lacZ/+}$, Fig. 2C). β-Galactosidase activity is detectable in developing PAs1 and 2, indicating that onset of Cre activity occurred at approximately the 10 somite stage (ss, indicated in lower right corner of each panel). Caudal ectoderm over the region that will form PAs3-6 is also stained prior to definitive arch formation (Fig. 2C, large red arrowheads).

Cells that express both *AP2α-IRESCre* and *Fgf8* were identified by staining for alkaline phosphatase (AP) activity in an *Fgf8*$^{AP/+}$; *AP2α*$^{IRES-Cre/+}$, 21 ss embryo. Analysis of whole mount and coronal sections demonstrates that AP is expressed specifically in the ectoderm of PAs 1-3 (Fig. 2D). This expression pattern reflects cells of the AP2α lineage that express *Fgf8*^{APR} (generated by *AP2α-IRESCre* activity), and defines the functionally relevant domains of *Fgf8* inactivation.

We confirmed that *AP2α-IRESCre* ablates Fgf8 throughout its ectodermal expression domains by comparing expression of GFP in *Fgf8*$^{GFP/+}$;*AP2α*$^{IRES-Cre/+}$ embryos versus *Fgf8*$^{GFP/+}$;*deleterCre* embryos (Fig. 2E, left and right panels, respectively). The *deleterCre* transgene is active in germ cells so *Fgf8*^{GFP} is recombined in all cells of the embryo from the earliest developmental stages (Schwenk et al., 1995). Therefore, GFP expression in *Fgf8*$^{GFP/+}$;*deleterCre* embryos depends only on the activity of the *Fgf8* locus. Importantly, *Fgf8*^{GFPR} expression in the PA ectoderm is the same whether it results from the action of *AP2α-IRESCre* or *deleterCre* (Fig.

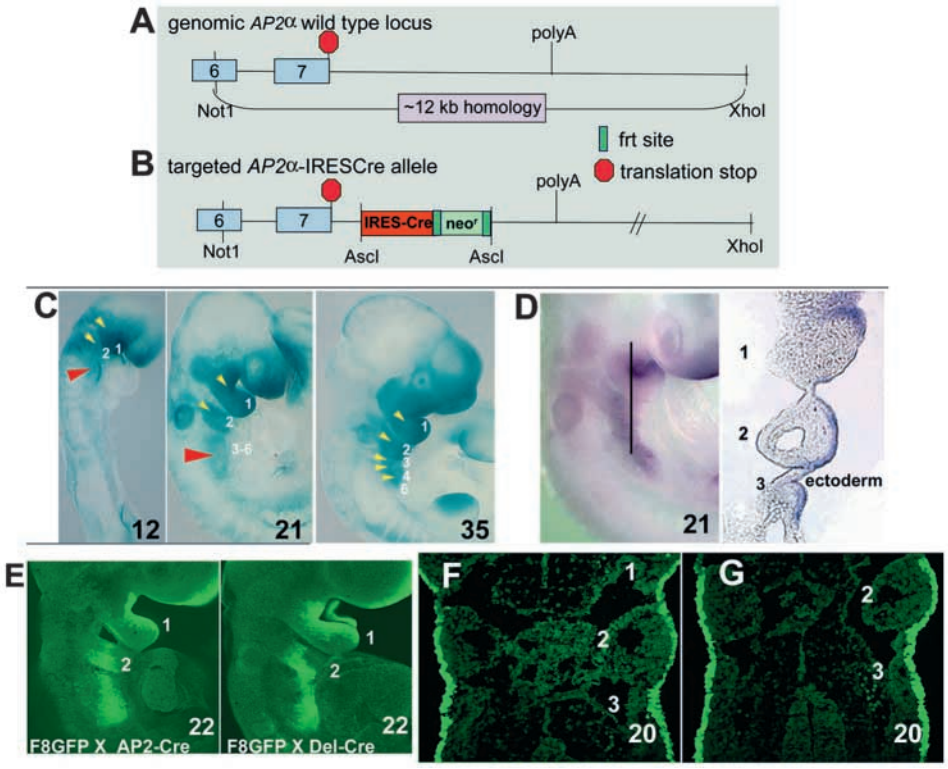

Fig. 2. The *Ap2α*-IRESCre driver ablates FGF8 in the developing pharyngeal arch (PA) ectoderm. (A) A 12 kb genomic fragment containing exons 6, 7, the 3′ UTR and polyadenylation signal from the *Ap2α* locus was used to generate the targeting vector for homologous recombination in ES cells. (B) The targeted allele contains the IRESCre cassette (see Materials and methods), positioned 198 bp 3′ of the translation stop in an engineered *Asc*I site. (C) *AP2α-IRESCre* was tested for Cre activity by crossing to the *Rosa26*^{lacZ} reporter strain. 12, 21 and 35 somite stage embryos, with the genotype *AP2α*$^{IRESCre/+}$*; Rosa26*$^{lacZ/+}$, were assayed for β-galactosidase activity (blue staining). Somite stages (ss) are labeled in the lower right corner of each panel and PAs are numbered. Blue staining, and both yellow and red arrowheads denote regions of Cre activity in the ectoderm of the PAs as they develop; Cre activity in the caudal ectoderm that will form PAs 3-6 is highlighted by the large red arrowhead in the 12 and 21 ss embryos. (D) Functionally relevant recombination of the *Fgf8*^{AP} conditional reporter allele in the developing PA ectoderm by the *AP2α-IRESCre* driver. A whole-mount, 21 ss *Fgf8*$^{AP/+}$*;AP2α*$^{IRESCre/+}$ embryo is shown in the left panel after assaying for alkaline phosphatase activity. The black line indicates the plane of the coronal section shown in the right panel. The ectoderm of developing PA 3, and that of PAs 1 and 2, are stained violet because of *Fgf8*^{APR} activity. Although *AP2α-IRESCre* is expressed in neural crest, the ectomesenchyme of the PAs is not stained because *Fgf8* is not expressed in these cells. (E) *AP2α-IRESCre* ablates *Fgf8* function throughout its expression domains in the PA ectoderm. Expression of *Fgf8*^{GFPR} after recombination with the *AP2α-IRESCre* (left panel) versus universal 'deleter' Cre driver (right panel) (Schwenk et al., 1995), was assessed by whole-mount anti-GFP immunohistochemistry of 22 ss, stage-matched embryos (ss in lower right corner). The domains of *Fgf8* inactivation resulting from the *AP2α-IRESCre* driver are the same ectodermal domains detected with the universal 'deleter' Cre. *Fgf8*^{GFPR} is expressed in caudal ectoderm that will form PAs 3-6. (F,G) Coronal sections through PAs 1 and 2, and the developing third arch region of a 20 ss embryo. *Fgf8*$^{GFP/+}$;AP2α$^{IRESCre/+}$ embryo (G) reveals *Fgf8*^{GFPR} expression throughout the ectoderm of the developing third arch and cleft.

2E). Although *Fgf8* is also expressed in the PA endoderm at this stage (discussed below), the endodermal domain of GFP expression in the *Fgf8*$^{GFP/+}$*;deleterCre* embryo (Fig. 2E, right panel) is obscured by overlying ectodermal signal. Coronal sections of a 20 ss *Fgf8*$^{GFP/+}$*; AP2α*$^{IRES\text{-}Cre/+}$ embryo (Fig. 2F,G) reveal that *AP2α-IRESCre* is not active in the endoderm, and that the ectoderm of PAs 1, 2 and developing PA3 express GFP.

All of these data provide confirm that in *Fgf8;AP2α-IRESCre* conditional mutants (*Fgf8*$^{GFP/null}$*; AP2α*$^{IRES\text{-}Cre/+}$), FGF8 is ablated specifically in the PA ectoderm.

hoxa3-IRESCre ablates FGF8 signaling from the PA endoderm and ectoderm

To simultaneously ablate *Fgf8* gene function in both the endoderm and ectoderm of PAs 3-6, we used the *hoxa3-IRESCre* driver (Fig. 3A,B). Lineage analysis of *hoxa3-IRESCre* in *hoxa3*$^{IRESCre/+}$*; Rosa26*$^{lacZ/+}$ embryos shows that *hoxa3-IRESCre* recapitulates the caudal to rostral progression of the endogenous *hoxa3* locus (Fig. 3C, 10-28 ss whole-mount panels). Previous reports described *hoxa3* expression in endoderm and mesenchyme of PAs3 and 4 (Manley and Capecchi, 1995), but we also found *lacZ* staining in the ectoderm of PAs 3-6 (see Fig. 3C, sectioned 20 ss and 23 ss embryos). Ectodermal *lacZ* staining is lighter than in mesenchyme (which may explain inability to detect this domain of *hoxa3* mRNA by in situ hybridization). Ectodermal expression was consistent in all embryos and was also confirmed using the *Fgf8*^{GFP} reporter allele.

To evaluate functionally relevant activity of *hoxa3-IRESCre* in *Fgf8*-expressing cells, we analyzed *Fgf8*^{GFPR} expression in *Fgf8*$^{GFP/+}$*; hoxa3*$^{IRESCre/+}$ coronally sectioned embryos (Fig. 3D) in comparison with *Fgf8*$^{GFP/+}$*;deleterCre* embryos (Fig. 3E). The relative planes of ventral and dorsal coronal sections are demonstrated by the black lines labeled v and d in the 20 ss whole mount in Fig. 3C. *Fgf8*^{GFPR} is clearly expressed in the endoderm and ectoderm of developing PAs 3-6, including pharyngeal pouches and clefts. At the 20 ss, ventral and dorsal sections (Fig. 3D, 20v and 20d, respectively) show *Fgf8*^{GFPR} expression throughout the PA3 endoderm, including the developing third pouch (3p), and ectoderm. By the 24 ss, *Fgf8*^{GFPR} expression is decreasing in the rostral endoderm of PA3, but persists in caudal endoderm and pouch (Fig. 3D, 24v and 24d, yellow arrowheads). At the 27 ss, GFP is detected throughout endoderm and ectoderm of PA4 as it forms. Remarkably,

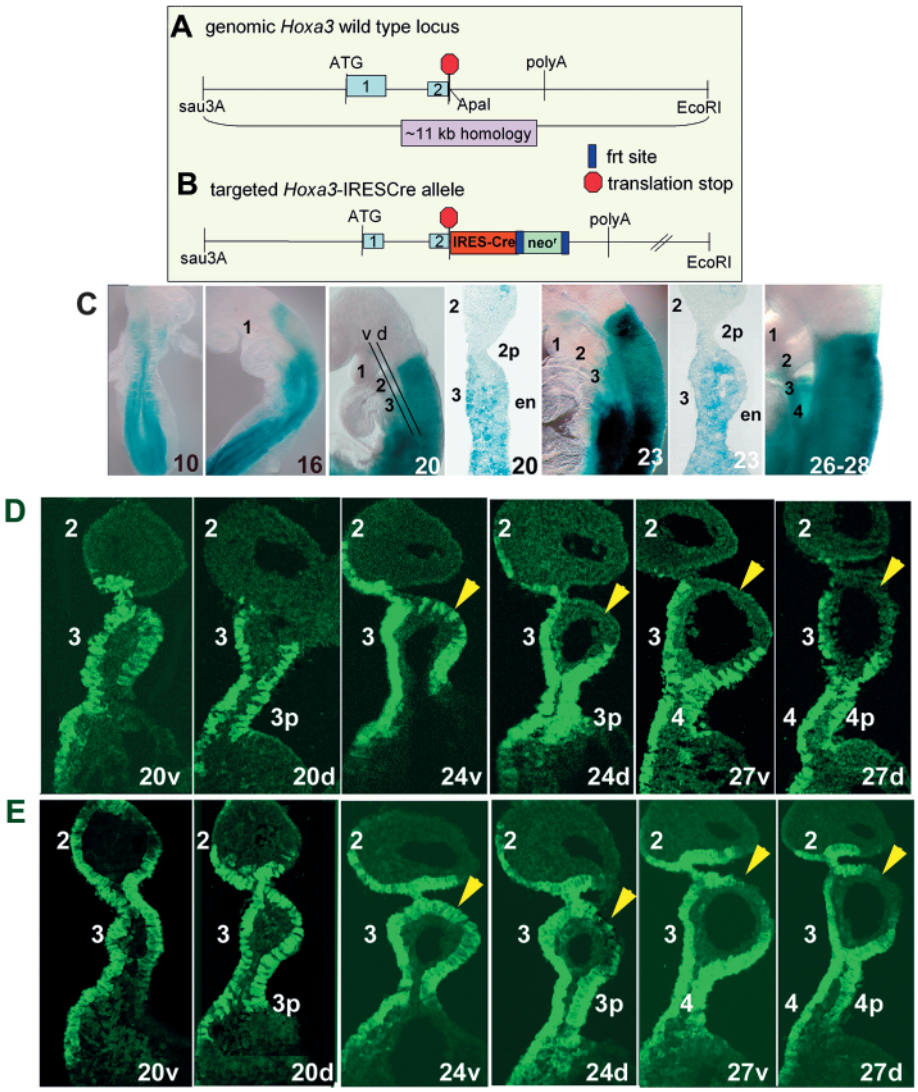

Fig. 3. *hoxa3-IRESCre* ablates *Fgf8* function in the third and fourth PA endoderm and ectoderm. (A) 11 kb of murine *hoxa3* genomic sequence extending from a 5′ *Sau3*AI site to an *Eco*RI site 3′ of the stop codon in exon 2 was used to create the targeting vector. (B) The targeted allele contains the IRESCre cassette (red box) inserted in an *Apa*I site four bases 3′ of the stop codon. Function of the *hoxa3-IRESCre* allele assayed with the *Rosa26*^{lacZ} reporter. (C) Whole-mount and sectioned preparations of *Rosa26*$^{lacZ/+}$; *hoxa3*$^{IRESCre/+}$ embryos stained for β-galactosidase activity (blue staining) at the 10, 16, 20, 23 and 26-28 ss reveal the caudal-to-rostral progression of *hoxa3-IRESCre* activity and anterior limit at the rhombomere 4/5 boundary and the anterior border of PA3. The relatively dorsal plane of the coronal sections through the PAs is demonstrated by the black line labeled d in whole-mount panel 20. These results demonstrate *hoxa3-IRESCre* activity in all three tissue layers of developing PAs 3-6. PAs are numbered; ss are noted in lower right corner of each panel. 2p, PA2 pouch; en, endoderm. (D,E) Functionally relevant recombination of *Fgf8*^{GFP} in the developing PA epithelia by *hoxa3-IRESCre* occurs throughout the *Fgf8* PA3-6 epithelial expression domains. (D) Coronal sections through the PAs of different stage *Fgf8*$^{GFP/+}$; *hoxa3*$^{IRESCre/+}$ embryos were assayed for GFP using fluorescent immunohistochemistry. Somite stages (ss) are labeled in the lower right corner of each panel followed by a letter indicating relative plane of each section within the arch of interest; v, ventral; d, dorsal (plane illustrated in Fig. 3C, whole-mount panel 20, black lines labeled v or d). PAs are numbered; 3p, PA3 pouch, etc. *Fgf8*^{GFPR} expression is initially detected throughout the epithelia of developing PA3 and then is lost from the rostral endoderm (yellow arrowheads, sections 24v, d and 27v, d). Because the *Rosa26*^{lacZ} reporter studies in Fig. 3C indicate that *hoxa3-IRESCre* is active throughout the endoderm of PA3 from the 20 ss, this loss of *Fgf8*^{GFPR} expression in rostral endoderm reflects a change in the *Fgf8* expression domain, not failure of *hoxa3-IRESCre* expression in these cells. (E) GFP expression was assayed in coronal sections of *Fgf8*$^{GFP/+}$; *deleterCre* embryos. Stage-matched embryos to those shown in D were assayed for GFP. Note that the expression of GFP from the globally recombined *Fgf8*^{GFPR} allele entirely recapitulates that seen in the PAs of *Fgf8*$^{GFP/+}$; *hoxa3*$^{IRESCre/+}$ embryos, including the loss of expression at later stages in the rostral endoderm of PA3 (yellow arrowheads, sections 24v,d and 27v,d). These studies confirm that *hoxa3-IRESCre* ablates *Fgf8* function throughout its PA epithelial expression domains from at least 20 ss. Labels are as noted for D.

the expression pattern of GFP was the same in *Fgf8*$^{GFP/+}$;*deleterCre* and *Fgf8*$^{GFP/+}$; *hoxa3*$^{IRESCre/+}$ embryos. Note that *Fgf8* is not expressed in PA mesenchyme (Fig. 2D,F,G; Fig. 3D,E).

In concert, the data in Fig. 3 clearly show that in *Fgf8*$^{GFP/null}$; *Hoxa3*$^{IRES\text{-}Cre/+}$ mutants (*Fgf8;hoxa3-IRESCre* mutants), FGF8 is ablated throughout its expression domains in endoderm and ectoderm of developing PAs 3-6. *hoxa3-IRESCre* activity is reproducibly present in the endoderm from the 18-19 ss, and from the 16 ss in the ectoderm (data not shown). Note that thymic and parathyroid epithelia arise from the third endodermal pouch, and that ‘cardiac’ neural crest migrates from rhombomeres 6-8 through PAs 3-6 into the OFT (Kirby et al., 1997; Kirby and Waldo, 1990; Kirby and Waldo, 1995). These are the relevant domains of *hoxa3-IRESCre* activity.

Phenotypes of *Fgf8* domain-specific conditional mutants

Ablation of FGF8 from the PA ectoderm causes vascular defects

The consequence of specifically ablating FGF8 in the PA ectoderm was determined by comparing *Fgf8;AP2α-IRESCre* ectodermal domain mutants (genotype *Fgf8*$^{GFP/null}$ or $^{AP/null}$; *AP2α*$^{IRES\text{-}Cre/+}$) with controls (genotypes *Fgf8*$^{+/+}$, *Fgf8*$^{AP/+}$, or *Fgf8*$^{+/null}$) and *Fgf8* hypomorphs (genotype *Fgf8*$^{APN/null}$) at multiple developmental stages using anatomic and molecular assays (Figs 4-7).

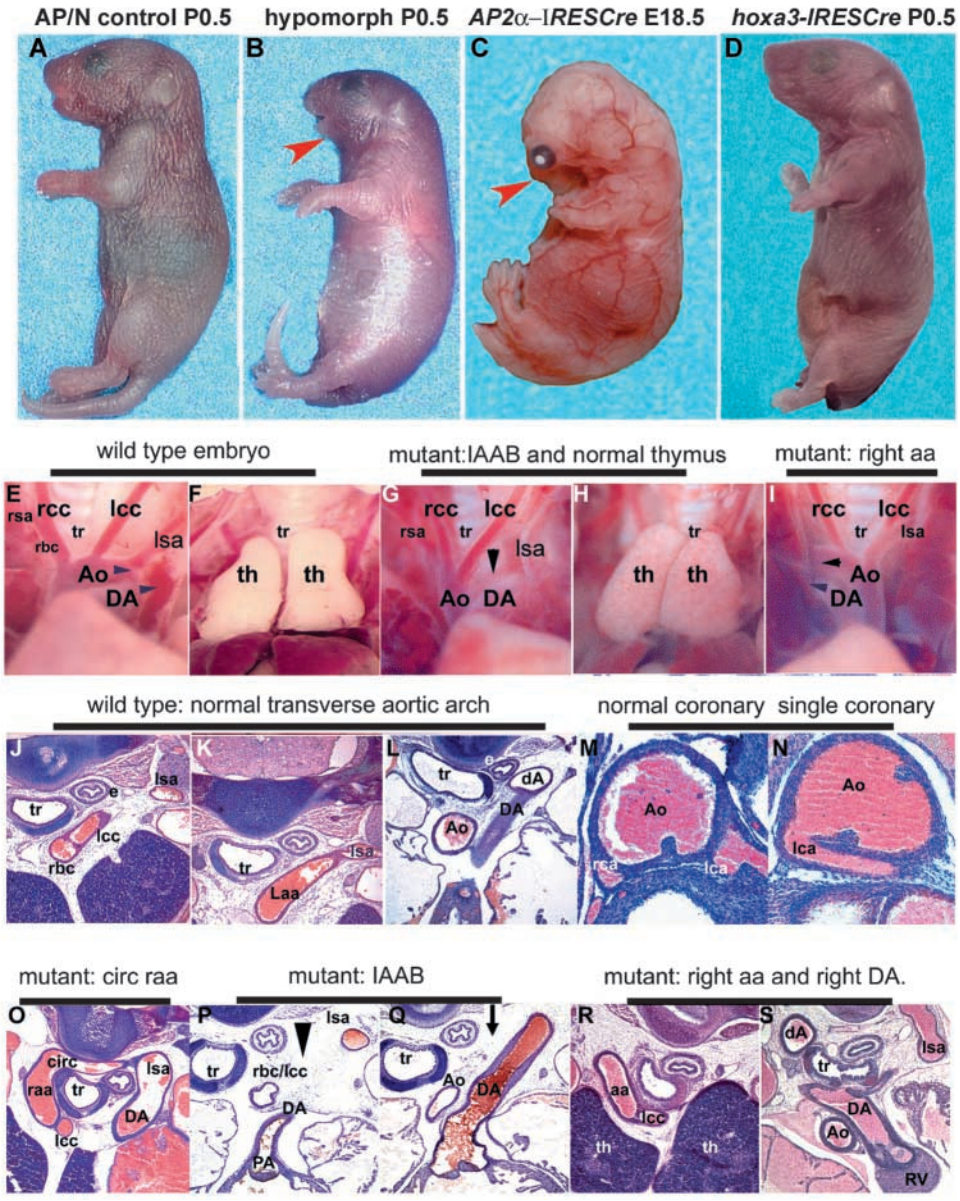

Fig. 4. Ablation of FGF8 in the PA ectoderm with *AP2α-IRESCre* reveals a unique and required role for FGF8 during PA vascular development, separate from its role in glandular and outflow tract development. (A-D) Gross morphology of perinatal control and mutant embryos. (A) *Fgf8*$^{AP/N}$ newborn control; note that in the absence of any source of Cre, embryogenesis occurs normally with only one functional, nonhypomorphic allele of *Fgf8*. (B) *Fgf8* newborn hypomorphic mutant (*Fgf8*$^{APN/N}$); the decrease in *Fgf8* mRNA produced by the *Fgf8*^{APN} allele cannot support normal development resulting in neonatal death, growth delay, edema, cyanosis, craniofacial malformations (red arrowhead) and cardiovascular defects. (C) *Fgf8/AP2α-IRESCre* E18.5 mutant; note absence of the lower jaw (red arrowhead) and bulging eyes, showing that complete ablation of FGF8 in PA1 results in a much more severe craniofacial defect than FGF8 deficiency in the hypomorph (red arrowhead). (D) *Fgf8/hoxa3-IRESCre* newborn has normal craniofacial development because Cre is not expressed anterior to PA3. (E-I) Thoracic dissections of control and *Fgf8/AP2α-IRESCre* mutant newborns. (E) Wild-type specimen with normal ascending aorta and left aortic arch (Ao, arrowhead), left ductus arteriosus (DA, arrowhead), right common carotid (rcc), left common carotid (lcc), right subclavian artery (rsa), left subclavian artery (lsa), trachea (tr); the right brachiocephalic artery (rbc) branches to form the rsa and rcc. (F) Normal bi-lobed thymus (th) in wild-type animal. (G) Removal of the thymus (see H) from an *Fgf8/AP2α-IRESCre* mutant reveals interrupted aortic arch type B (IAAB, no transverse aortic arch, black arrowhead), a left DA and an abnormal isolated lsa. (H) The same mutant shown in G has a normal thymus. *AP2α-IRESCre*-mediated ablation of FGF8 separates vascular from outflow tract and pharyngeal gland defects that result from global *Fgf8* deficiency. (I) *Fgf8*/*AP2α-IRESCre* mutant after removal of the thymus; in this case there is a right aortic arch (Ao, arrowhead) and a right DA (arrowhead). (J-L) Transverse sections of a wild-type animal showing the normal progression (slides shown from rostral to caudal) of the head and neck vessels arising from the transverse left aortic arch. (J,K) Normal junction of rbc and lcc to lsc to form the Laa. (L) Normal ascending Ao and junction of DA to descending aorta (dA). (M) Normal right and left coronary arteries (rca, lca) arising from the left and right cusps of the aortic valve. (N-S) *Fgf8*/*AP2α-IRESCre* mutants have multiple vascular anomalies caused by abnormal formation of the fourth PAAs. (N) Single coronary artery with abnormal origin of lca from right cusp of aortic valve; the rca branches off this vessel in a more caudal location. (O) Circumflex right aa (circ raa) joining lsa after a retroesophageal route; the DA also joins the lsa to form a left descending Ao (not shown). (P,Q) IAAB: the ascending aorta gives rise to the junction of the rbc and lcc (see also E). The transverse aortic arch (P, arrowhead) and descending Ao (Q, arrow) are absent, resulting in an isolated lsa that only connects with the DA (Q) to form the left descending aorta (not shown); this lesion is lethal. (R,S) A different *Fgf8*/*AP2α-IRESCre* mutant with right aortic arch: the lcc joins the rbc to form the transverse region of the right-sided arch (aa). A right DA, right descending aorta (dA) and an aberrant lsa are also seen in this mutant (S).

Fgf8 hypomorphs survive to birth, but 100% die in the neonatal period with a complex phenotype that includes growth delay, cyanosis, craniofacial, cardiovascular and pharyngeal gland defects (Fig. 4B). Hypomorphs have severe cardiac OFT septation and alignment defects. Their vascular abnormalities result from abnormal development of the fourth pharyngeal arch artery (PAA) (Abu-Issa et al., 2002; Frank et al., 2002).

By contrast, only 75% of *Fgf8;AP2α-IRESCre* mutants survive to birth and the rest die postnatally due to lethal vascular defects in 30% and severe craniofacial malformation in 100%. The craniofacial defect results from complete

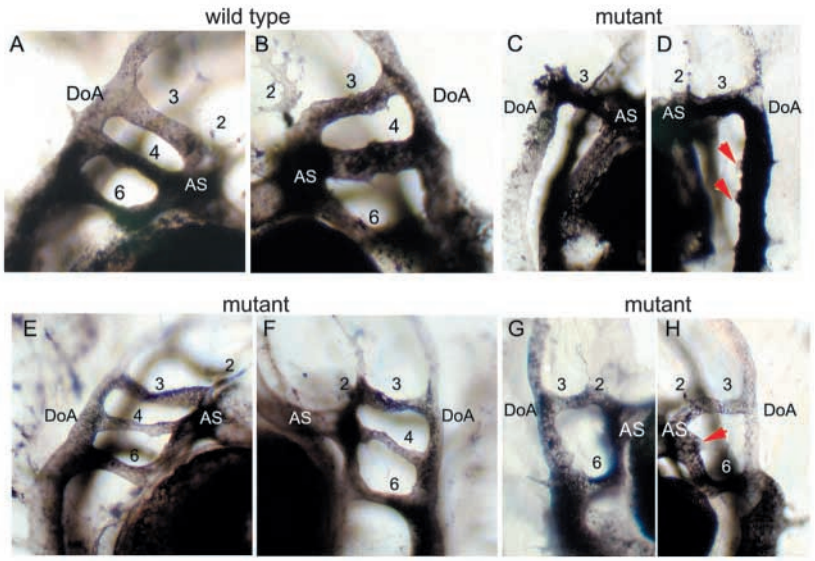

Fig. 5. Pharyngeal arch artery defects in *Fgf8* domain-specific mutants at E10.5. Stage-matched embryos are shown photographed at the same magnification. (A,B) Ventrolateral views of the right (A) and left (B) sides of an ink injected E10.5 control embryo. Remodeling toward a left dominant system is already evident. Pharyngeal arch arteries (PAAs) are numbered, the dorsal aorta and aortic sac are labeled (DoA, AS respectively). (C,D) An *Fgf8*/*AP2α*-IRESCre mutant with bilateral aplasia of the fourth and sixth PAAs. The third PAA is abnormally enlarged and provides blood flow from the heart to the DoA (see also Fig. 7, rows K, L). There are sprouts from the DoA visible on the left side (red arrowheads). (E-H) *Fgf8*/*AP2α*-IRESCre mutants with bilateral hypoplasia of the entire PAA system (E,F), or aplasia of the fourth PAAs (G,H); the red arrowhead highlights a sprout from the AS on the left side.

Table 1. Cardiovascular phenotypes of *Fgf8* domain-specific mutants: sectioned specimens at E18.5

	Phenotype						
Genotype	Normal	IAAB	Circumflex/ RAA	RERSCA/abnormal SCA	Coronary artery anomaly*	Bicuspid aortic valve	Other
AP/+ or +/N (*n*=40)	40 (100%)	0	0	0	0	0	0
AP/N (*n*=15)	15 (100%)	0	0	0	0	0	0
AP/N; *AP2α*-ICre (*n*=24)	1 (5%)	7 (30%)	3 (13%)	Nineteen associated (80%), four isolated (17%)	11 (46%)	0	4 (16%)
AP/N; *hoxa3*-ICre (*n*=33)	2 (6%)	5 (15%)	3 (9%)	Seventeen associated (52%), five isolated (15%)	18 (55%)	7 (23%)	4 (13%)
P value (*Ap2α* versus *hoxa3* mutants)†	NS	NS	NS	0.05	NS	<0.02	NS

IAAB, interrupted aortic arch type B; circumflex/RA, circumflex right aortic arch or right aortic arch; RERSCA/abnormal SCA, retroesophageal right subclavian artery, abnormal subclavian branching, including right and/or left subclavian arteries.

*Majority in all genotypes was single coronary off right anterior cusp.

†Fisher's exact test, two-tailed.

Some category numbers exceed the total number examined because of multiple phenotypes in single animals.

ablation of FGF8 in PA1 (Fig. 4C). The pharyngeal phenotype is detected as early as E9.5 as severe PA1 hypoplasia and hypoplasia and fusion of more caudal PAs (data not shown).

The fourth PAAs form between E9.5-10.0 (25-29 ss); the right fourth PAA forms the proximal right subclavian artery, while the left fourth PAA becomes the aortic arch between the left common carotid and left subclavian arteries (the segment of aorta missing in IAAB). Ninety-five percent of *Fgf8*;*AP2α-IRESCre* mutants have vascular defects at birth resulting from abnormal formation of the fourth PAAs (Fig. 4G,O-S; Fig. 5; Tables 1 and 2). Thirty percent of *Fgf8*;*AP2α-IRESCre* E18.5 conditional mutants have the postnatally lethal vascular malformation, interrupted aortic arch type B (IAAB, Fig. 4G,P,Q). In addition to IAAB and subclavian artery anomalies, we observed circumflex right aortic arch (RAA, Fig. 4O) and RAA with right ductus arteriosus (Fig. 4E,R,S) in these mutants; defects also attributable to failed left PAA4 formation.

To evaluate fourth PAA formation in these mutants, we performed ink injections in E10.5 embryos. Ninety-five percent of *Fgf8*;*AP2α-IRESCre* embryos have abnormal fourth PAA formation: 33% display bilateral aplasia of the fourth and sixth PAAs, a phenotype we did not observe in *Fgf8* hypomorphs (Frank et al., 2002). The incidence of bilateral aplasia of PAAs 4 and 6 at E10.5 (33%), compared with survival of mutants to birth (75%), reveals that some embryos with this lesion at E10.5 survive. Thirty-three percent of these mutants display bilateral PAA4 aplasia (Fig. 5, Table 2). Recovery of the fourth and/or sixth PAAs by vascular remodeling was noted in some E11.5 mutants (data not shown).

Overall, the incidence of defects attributable to abnormal fourth PAA formation, such as IAAB, RAA or aberrant subclavian artery, is the same in *Fgf8* hypomorphs and *Fgf8*;*AP2α-IRESCre* mutants. However, the severity of the defects at E10.5 resulting from complete ablation of FGF8 in the PA ectoderm is much greater in *Fgf8*;*AP2α-IRESCre* mutants when compared with the globally deficient hypomorphs. This indicates that the pharyngeal FGF8 ectodermal domain has required function(s) during PAA4 vasculogenesis.

We have previously shown that PAA4 vasculogenesis is specifically disrupted in *Fgf8* hypomorphs: endothelial cells (ECs) are specified and differentiated in the fourth PA as they

Table 2. Pharyngeal arch artery (PAA) development in *Fgf8/AP2α*-Cre mutants: assessed by India ink injection at E10.5-11

Genotype	Phenotype					
	Normal	Aplastic PAAs 4 and 6	Aplastic PAA 4 bilateral	Hypoplasia PAA 4 bilateral	Hypo/aplastic PAA 4, L	Hypo/aplastic PAA 4, R
AP/+ (*n*=41)	41 (100%)	0	0	0	0	0
AP/+; *AP2α*-ICre (*n*=40)	40 (100%)	0	0	0	0	0
AP/N (*n*=38)	24 (64%)	0	0	0	8 (21%)*	6 (16%)†
AP/N; *AP2α*-ICre (*n*=37)	2 (6%)	12 (33%)‡	12 (33%)	4 (12%)	4 (12%)§	3 (8%)¶

*Four embryos had left PAA, four had hypoplasia and 4 had aplasia (nonpatent to ink).

†Most of these are probably attributable to normal remodeling to the left-side dominant system, which we have observed to occur as early as E10.5 in the C57Bl6 background; one embryo had an aplastic right PAA 4.

‡Eleven embryos had bilateral aplasia of PAAs 4 and 6; two embryos had aplasia of PAAs 4 and 6 on the right with PAA 4 aplasia on the left.

§Three embryos were aplastic.

¶One aplastic.

These results indicate that the ectodermal domain of FGF8 is specifically required for correct formation of the fourth pharyngeal arch artery (PAA). Remodeling and recovery from these fourth PAA defects results in the array of vascular defects seen in *Fgf8*/*Ap2α*-Cre mutants at birth.

Table 3. Glandular phenotypes of *Fgf8* domain-specific mutants: sectioned specimens at E18.5

Genotype	Normal thymus	Ectopic thymus	Hypoplastic thymus	Normal parathyroid glands*	Ectopic parathyroid glands	Hypoplastic parathyroid glands	Absent parathyroid glands
AP/+ or +/N (*n*=40)	38 (95%)	2 (5%)	0	76 (100%)	3 (4%)	1 (1%)	0
AP/N (*n*=15)	15 (100%)	0	0	30 (100%)	0	0	0
AP/N; *AP2α*-ICre (*n*=24)	22 (92%)	2 (8%)	0	44 (92%)	2 (4%)	2 (4%)	0
AP/N; *hoxa3*-ICre (*n*=33)	10 (31%)	17 (51%)†	13 (41%)‡	20 (32%)	31 (48%)	38 (58%)	18 (28%)§
P value *Ap2α* versus *hoxa3* mutants	0.05	<0.001	<0.001	<0.001	<0.001	<0.001	<0.001

*Note individual glands were scored.

†Eight animals had isolated ectopic lobes; nine had ectopic lobes in combination with hypoplasia of one or both lobes. Sixty-eight percent had markedly abnormal migration and/or hypoplasia of thymic tissue.

‡Five animals had isolated hypoplastic lobes; nine had hypoplastic lobes in combination with ectopy of one or both lobes.

§67% were abnormal overall. Ten animals had bilaterally normal parathyroids; seven had unilateral defects and 15 had bilateral defects. As parathyroids may be found embedded in, posterior-lateral to, or anterior-lateral to the thyroids in normal animals at this age, ectopy was scored only if a gland was estimated to be less than 50% the size of a normal gland.

These data indicate that the pharyngeal endodermal domain of FGF8 has a required separable role in thymic and parathyroid morphogenesis, and that the ectodermal domain does not contribute to these processes.

express the VEGF receptor, Flk1 and the cell adhesion molecule PECAM (Cleaver and Krieg, 1999). However, the ECs fail to organize into primitive vascular tubes (Frank et al., 2002). To evaluate vasculogenesis in *Fgf8;AP2α-IRESCre* mutants, we examined whether migration and specification of ECs in the fourth PA proceeds normally. Flk1/PECAM-expressing cells were detected in hypoplastic fourth PAs of *Fgf8;AP2α-IRESCre* mutants at the 25-27 ss (during PAA4 formation) in clusters that are indistinguishable from controls, *Fgf8* hypomorphs, or *hoxa3-IRESCre* mutants (discussed below, and data not shown). However, in all classes of *Fgf8* mutants at the 35-37 ss, ECs in PAA4 remain disorganized and fail to form primitive vascular tubes, long after this vessel is patent and pericyte recruitment is under way in controls (data not shown) (Frank et al., 2002). Thus, migration and early differentiation of PAA4 ECs occurs normally in the absence of FGF8, but subsequent vascular organization fails.

Remarkably, and unlike *Fgf8* hypomorphs, *Fgf8;AP2α-IRESCre* mutants have normal OFT development: that is, alignment, septation and rotation of the aortic and pulmonary arteries are normal. In the mutant shown in Fig. 4G, the aorta and ductus arteriosus/pulmonary artery are normally aligned and septated, but the mutant has the IAAB vascular defect. *Fgf8;AP2α-IRESCre* mutants also have coronary artery anomalies (Fig. 4M,N), in isolation or associated with other vascular defects (Table 1).

In further contrast to *Fgf8* hypomorphs, *Fgf8;AP2α-IRESCre* mutants have normal thymic and parathyroid glands (Fig. 4H, Table 1, Table 3).

The presence of vascular phenotypes and the absence of OFT or glandular defects in *Fgf8;AP2α-IRESCre* mutants reveal a distinct functional and anatomic FGF8 signaling domain that is essential for PAA formation and separable from the FGF8 expression domains required for OFT and pharyngeal gland development.

Ablation of FGF8 from the PA endoderm causes glandular and aortic valve defects

We used the *hoxa3-IRESCre* driver to ablate FGF8 from both the endoderm and ectoderm of PAs 3-6 as they develop. In marked contrast to both *Fgf8* hypomorphs and *Fgf8;AP2α-IRESCre* mutants, all *Fgf8;hoxa3-IRESCre* mutants survive to birth and most survive beyond the neonatal period. These mutants have normal craniofacial morphology because *Fgf8* is intact anterior to PA3 (Fig. 4D). Thirty percent of *Fgf8;hoxa3-IRESCre* mutants die as neonates because of the same lethal

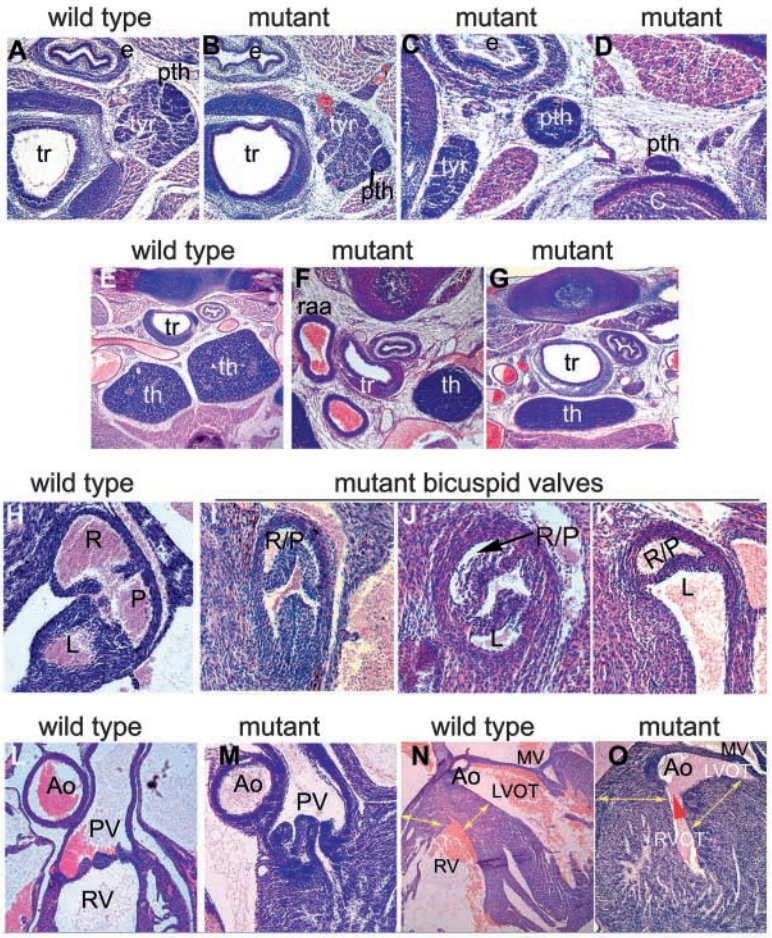

Fig. 6. Ablation of FGF8 in the PA endoderm and ectoderm by *hoxa3-IRESCre* reveals that endodermal domain-specific FGF8 activity is required for thymic, parathyroid and aortic valve formation. (A) Sections through neck of E18.5 control. Note the large parathyroid gland (pth) embedded in posterior-lateral aspect of thyroid (tyr). e, esophagus; tr, trachea. (B-D) Parathyroid ectopy and/or hypoplasia in *Fgf8/hoxa3-IRESCre* mutants. c, clavicle. (E) Wild-type control with normal bi-lobed thymus. (F,G) Thymic hypoplasia and migration defects in *Fgf8/Hoxa3-IRESCre* mutants. (F) Hypoplastic left thymus in association with a right aortic arch (raa). (G) Monolobed ectopic gland. (H) Cross-section of normal aortic valve in control animal, anterior is towards the left; note three cusps: right (R), left (L), posterior (P). (I-K) Bicuspid aortic valves in *Fgf8/Hoxa3-IRESCre* mutants. (L) Cross-section through the right ventricular outflow tract of a control embryo showing the relationship of the aorta (Ao), pulmonary valve (PV) and right ventricle (RV). (M-O) Sections through an animal with Tetralogy of Fallot (TOF). (M) Dysplastic PV and severe subvalvar and infundibular stenosis. (N) Cross-section of the left ventricular outflow tract (LVOT), right ventricle (RV) and intact ventricular septum in a wild type animal; there is continuity between the aortic (Ao) and mitral (mv) valves. Note thickness of right ventricular free wall and ventricular septum (yellow bidirectional arrows); the heart is fixed in late systole (mitral valve is closed). (O) The mutant displays overriding aorta (both the right and left ventricular outflow tracts empty through the aortic valve), right ventricular hyperplasia with marked increase in thickness of the right ventricular wall and ventricular septum (yellow bidirectional arrows, heart in late systole), and a large membranous ventricular septal defect (red arrowhead).

cardiovascular malformations described in *Fgf8;AP2α-IRESCre* (Table 1 and below).

Notably, *Fgf8;hoxa3-IRESCre* mutants display thymic ectopy and hypoplasia and parathyroid ectopy, hypoplasia and aplasia (Table 3, Fig. 6A-G). Parathyroid and thymic epithelia are derived from the anterior and posterior third pouch endoderm, respectively. The incidence of abnormal thymic and parathyroid development in *Fgf8;hoxa3-IRESCre* mutants (Table 3) was comparable with that of *Fgf8* hypomorphs (Frank et al., 2002). However, the severity of these defects in *hoxa3-IRESCre* mutants was less than in globally deficient hypomorphs because no *hoxa3-IRESCre* mutants had bilateral thymic or parathyroid aplasia, which occurred frequently in *Fgf8* hypomorphs. Fourth pouch-derived thyroid C-cells were detected normally in *Fgf8;hoxa3-IRESCre* mutants, *Fgf8* hypomorphs and controls, as assessed by anti-calcitonin immunohistochemistry (data not shown). Notably, glandular defects are not seen in *Fgf8;AP2α-IRESCre* mutants (Fig. 4G, versus Fig. 6A-G, Table 3).

As FGF8 is also ablated in the ectoderm of PAS 3-6 in *Fgf8;hoxa3-IRESCre* mutants, it was not surprising to find the same PAA and coronary vascular defects in these mutants seen in *Fgf8;AP2α-IRESCre* mutants (see above and Table 1). However, it is quite remarkable that ablation of FGF8 in both the endoderm and ectoderm in *Fgf8;hoxa3-IRESCre* mutants does not increase either incidence or severity of PAA or coronary vascular defects at any developmental stage (Tables 1, 2, 4). The same defect in vascular tube formation in the fourth PA described in *Fgf8* hypomorphs and *Fgf8;AP2α-IRESCre* mutants was also detected in *Fgf8;hoxa3-IRESCre* mutants. These findings confirm that the ectodermal domain of FGF8 is specifically required for normal PAA and coronary vascular development.

Twenty-three percent of *Fgf8;hoxa3-IRESCre* mutants (Fig. 6I-K, Table 1) had bicuspid aortic valves (BAV). By contrast, BAV was not seen in *Fgf8;AP2α-IRESCre* mutants and was found in *Fgf8* hypomorphs in association with severe OFT lesions. Given the high frequency of BAV in *Fgf8;hoxa3-IRESCre* mutants, we were surprised to find that only 1/33 of these mutants had severe perturbation of OFT septation and alignment (Tetralogy of Fallot and BAV, Fig. 6J,M,O).

The glandular and valvar phenotypes of *Fgf8;hoxa3-IRESCre* mutants indicate that the FGF8 endodermal domain ablated by *hoxa3-IRESCre* has distinct functional roles in pharyngeal and aortic valve development.

Differential survival of neural crest is not the mechanism for the distinct phenotypes of *Fgf8* hypomorphic and domain-specific, *AP2a-IRESCre* ectodermal and *Fgf8;hoxa3-IRESCre* mutants

We previously reported that neural crest (NC) cells in developing PAs 3-6 undergo abnormal apoptosis at the 25-29 ss in *Fgf8* hypomorphs (Frank et al., 2002). As the cardiovascular features of hypomorphs recapitulate those of NC-ablated chicks (Kirby et al., 1985), we hypothesized that

Table 4. Pharyngeal arch artery (PAA) development in *Fgf8*/*hoxa3*-IRESCre mutants: assessed by India ink injection at E10.5

Genotype	Normal	Aplastic PAAs 4 and 6	Aplastic PAA 4 bilateral	Hypoplasia PAA 4 bilateral	Hypo/aplastic PAA 4, L	Hypo/aplastic PAA 4, R
AP/+ (*n*=19)	19 (100%)	0	0	0	0	0
AP/+; *hoxa3*-ICre (*n*=19)	19 (100%)	0	0	0	0	0
AP/N (*n*=17)	11 (65%)	0	0	0	1 (6%)*	6 (34%)†
AP/N; *hoxa3*-ICre (*n*=18)	0	5 (24%)‡	6 (28%)	4 (20%)§	3 (15%)¶	3 (15%)**

*Severe hypoplasia.

†Most of these are probably attributable to normal remodeling to the left-side dominant system, which we have observed to occur as early as E10.5 in the C57Bl6 background; one embryo had right PAA 4 aplasia.

‡Three embryos had bilateral PAA 4 and 6 aplasia; two had PAA 4 and 6 aplasia on the right with PAA 4 aplasia on the left.

§Two embryos had severe hypoplasia of the entire left sided system.

¶One embryo was aplastic.

**All three embryos were aplastic.

These results show that there is no increase in incidence or severity of fourth PAA defects when FGF8 is ablated from the endodermal domain in addition to the ectodermal domain, and support our conclusion that the ectoderm supplies the required signal for fourth PAA vasculogenesis.

the high incidence of severe OFT defects in hypomorphs (85%), resulted from abnormal NC survival in PAs 3-6 prior to entering the OFT (Frank et al., 2002). As we have now demonstrated that differential ablation of FGF8 in PA ectoderm and endoderm separates vascular from glandular and OFT defects, we questioned whether domain-specific mutants would display unique patterns of NC apoptosis. Therefore, we compared apoptosis in all three classes of *Fgf8* mutants by whole-mount TUNEL. We detected the same abnormal areas of apoptosis in PA3 and developing PAs 4 and 6 in *Fgf8* hypomorphs and domain-specific mutants (Fig. 7A-H, compare white circled regions and white arrowheads in controls with yellow arrowheads in mutants). Note that similar domains of normal (transient, stage specific) apoptosis are present in the otocysts of all embryos, indicating appropriate stage matching.

These observations were confirmed by assaying for apoptosis and expression of the transcription factor Ap2α (labels NC) using double fluorescent immunohistochemistry on serial cryosections of 25 ss embryos (Fig. 7I-L). Minimal NC apoptosis was detected in controls (Fig. 7, row I), whereas all three mutant classes had large abnormal domains of apoptosis in NC migrating from rhombomeres 6-8 into the lateral regions of PA3, and developing PAs 4 and 6 (yellow arrowheads). The hypomorph shown had hypoplastic third PAAs (Fig. 7, row J) and large domains of abnormal apoptosis. Note the abnormally large third PAA in *Fgf8;AP2α-IRESCre* and *Fgf8*;*hoxa3-IRESCre* mutants (Fig. 7, rows K and L, respectively; white asterisks mark third PAAs); consistent with abnormal persistence and enlargement of the third PAA in mutants when the fourth PAAs do not form (see Fig. 5C).

Discussion

Dissecting functions of individual *Fgf8* expression domains

Mice with globally decreased FGF8 signaling throughout embryogenesis (*Fgf8* hypomorphs) display severe cardiovascular and pharyngeal defects, and phenocopy the cardiovascular, craniofacial and glandular abnormalities seen in humans with del22q11 syndromes (Abu-Issa et al., 2002; Frank et al., 2002). We previously postulated that *Fgf8* may play a role in the developmental dysfunction that results in human del22q11 phenotypes (Frank et al., 2002). This hypothesis has subsequently been supported by a description of a genetic interaction between *Fgf8* and *Tbx1*, a gene located within the del22q11 region (Vitelli et al., 2002).

To determine if local FGF8 signals in the arches contribute to normal pharyngeal and cardiovascular development, and to evaluate which of the many potentially relevant *Fgf8* expression domains might be responsible for different aspects of *Fgf8* hypomorphic pharyngeal and cardiovascular phenotypes, we generated a system of nonhypomorphic *Fgf8* conditional reporter alleles and domain-specific Cre-recombinase drivers. Appropriate combinations of these alleles in murine embryos allowed us to differentially ablate FGF8 in distinct temporospatial expression domains in the developing PAs.

AP2α-IRESCre unequivocally ablates FGF8 throughout its expression domains in PA ectoderm from the time of PA formation, at least by the 10-somite stage. By contrast, *hoxa3-IRESCre* is active in all three germ layers of developing PAs 3-6 from the 16 ss in the ectoderm and the 18-19 ss in the endoderm.

These detailed expression analyses allowed us to determine the precise location and timing of overlap between *Fgf8* expression and *Cre* expressed by the different temporospatially restricted drivers. This is crucial to discerning how ablation of FGF8 in a given domain relates to the distinct phenotypes obtained by domain-specific conditional mutagenesis and in comparison with the complex *Fgf8* hypomorphic phenotype.

Domain-specific phenotypes reveal distinct, essential functions of local FGF8 signals in cardiovascular and pharyngeal development

Fgf8 domain-specific mutants display vascular, coronary artery, aortic valve and pharyngeal gland phenotypes due to loss of specific, local FGF8 signals from separate expression domains in the PA ectoderm and endoderm.

Our *Fgf8* allelic series and conditional mutagenesis system reveals a remarkable dosage sensitivity of regional vascular development to FGF8 levels in the caudal PA ectoderm. This domain of expression is required for normal formation of the fourth (and frequently sixth) PAA (Tables 1, 2, Figs 4, 5). Although the overall incidence of PAA4-related vascular defects (IAAB, RAA, subclavian artery anomalies) was the

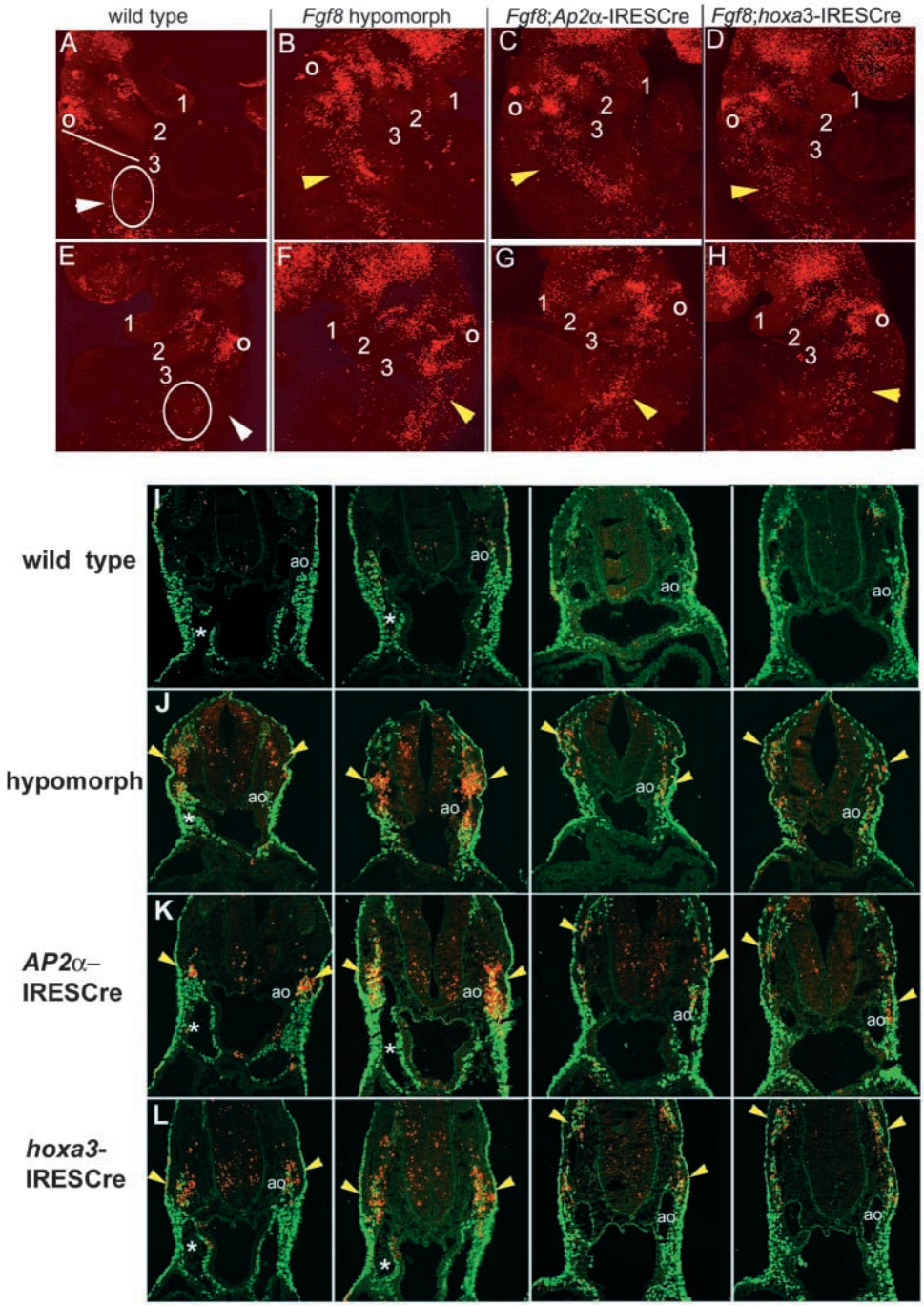

Fig. 7. TUNEL analysis of whole-mount and sectioned preparations specimens reveals similar patterns of abnormal neural crest apoptosis in *Fgf8* hypopmorphs, *Fgf8/AP2α-IRESCre* and *Fgf8/HoxA3-IRESCre* mutants. Both experiments were repeated three times with comparable results. The whole-mount experiment was performed with all embryos in the same tube; the sectioned specimens were all processed simultaneously. PAs are numbered; o, otocyst. (A-H) Right and left views of 25-26 ss stage-matched embryos. (A,E) A wild-type embryo has minimal apoptosis in the region of PAs 3-6 (white ovals, white arrowhead). The white line indicates plane of section for fluorescent immunohistochemical analysis shown in I-L. (B,F) An *Fgf8* hypomorph replicates our previous finding of abnormal domains of apoptosis in PAs 3-6 (yellow arrowheads) (Frank et al., 2002). (C,G) *Fgf8/AP2α-IRESCre* and (D,H) *Fgf8/hoxa3-IRESCre* mutants have increased NC apoptosis in the same regions noted in the hypomorph (yellow arrowheads). (I-L) Fluorescent immunohistochemistry was performed cryosectioned 25 ss, stage-matched control versus hypomorphic and domain-specific mutants using a combination of anti-AP2α/FITC (green fluorescence) to detect neural crest cells (NC) and TUNEL/Texas red (red fluorescence). Embryos were sectioned transversely in parallel with the third PA (see white line in A). Each row shows a representative section from a single embryo, proceeding from anterior to posterior through the post-otic region (from the third PAA to the developing fourth and sixth arch region). Sections were carefully matched to represent the same region of each embryo in each column, taking into consideration the profoundly perturbed anatomy and severe pharyngeal hypoplasia of *Fgf8* hypmorphic and *Fgf8/AP2α-IRESCre* mutants. White asterisks indicate the third PAA in parallel (not present in all sections), yellow arrowheads indicate regions of abnormal apoptosis and dying NC. The dorsal aorta is labeled (ao). (I) A control embryo has minimal apoptosis in NC migrating into the third PA or region of the developing fourth and sixth PAs. (J) An *Fgf8* hypomorph has large domains of abnormal apoptosis. Double-labeled NC are migrating from rhombomere 6 into the lateral third arch. Note that the pharynx is poorly segmented and that the PAs and third PAA are hypoplastic. (K) *Fgf8/AP2α-IRESCre* and (L) *Fgf8/hoxa3-IRESCre* mutants have NC apoptosis in the same domains as the hypomorph. In these examples, the third PAA is pathologically enlarged (see also Fig. 5C,D).

same in *Fgf8;AP2α-IRESCre* mutants and FGF8-deficient hypomorphs, the severity of PAA defects at E10.5 was much greater in *Fgf8;AP2α-IRESCre* mutants because of complete absence of FGF8 in the PA ectoderm from the earliest stages of PA formation. *hoxa3-IRESCre* mutants had (statistically) the same incidence and severity of PAA and coronary vascular defects as *Fgf8;AP2α-IRESCre* mutants, in spite of the fact that FGF8 was ablated in both the PA endoderm and ectoderm (Tables 1, 2, 4). Ablation of FGF8 with a *Tbx1Cre* transgene that is active in early endoderm and precardiac mesoderm (but not in arch ectoderm) results in OFT and glandular defects, but no fourth PAA-related vascular defects (J. Epstein, personal

communication). These observations indicate that FGF8 signaling from PA ectoderm is critical for normal PAA4 development and that the vascular defects seen in all classes of *Fgf8* mutants are attributable to FGF8 deficiency in the PA ectoderm.

By contrast, FGF8 ablation from the endoderm of PAs 3-6 in *Fgf8*; *hoxa3-IRESCre* mutants results in thymic, parathyroid and BAV defects. Thus the FGF8 endodermal domain makes important and distinct contributions to development of these structures. Thyroid, parathyroid and thymic epithelial cells are derived from pharyngeal pouch endoderm; these glands initially have a NC component, and interactions between NC and endoderm play an important role in early thymic and parathyroid development (Auerbach, 1960; Bockman and Kirby, 1984; Graham, 2001; Graham and Smith, 2001; LeDouarin and Jotereau, 1975; LeLievre and LeDouarin, 1975). Because FGF8 is ablated from both epithelial layers of the third pouch/cleft of *Fgf8*;*hoxa3-IRESCre* mutants, it is possible that glandular hypoplasia and ectopy in these mutants represents a combined effect of absence of FGF8 in both domains. This is unlikely given that the glandular hypoplasia and ectopy resulting from complete ablation of FGF8 in *hoxa3-IRESCre* mutants is less severe when compared with the frequent glandular aplasia seen in *Fgf8* hypomorphs. It is likely that an earlier endodermal FGF8 domain has a crucial influence on the earliest precursors of these glands. Indeed, the aforementioned *Fgf8*;*Tbx1Cre* mutants have thymic aplasia (J. Epstein, personal communication).

Fgf8 mutants reveal a role for neural crest in PA and coronary vascular development

The same regions of abnormal NC apoptosis are observed in the PAs of all classes of *Fgf8* mutants. Importantly, the only abnormal phenotypes common to these different mutants are PAA4-derived defects and coronary vascular anomalies. We hypothesize that signaling between NC-derived ectomesenchyme and endothelial cells (ECs) is required for normal PA vascular development prior to differentiation of NC into the vascular smooth muscle cells (VSMC) and pericytes supporting the PAAs. This signaling may be perturbed by abnormal death of NC migrating from rhombomeres 6-8 into and through PAs 3-6 in *Fgf8* mutants. Disruption of EC/ectomesenchymal interactions may contribute to both the PAA and coronary vascular defects seen in all classes of *Fgf8* mutants in our series.

Approximately 50% of *Fgf8;AP2α-IRESCre* and *Fgf8;hoxa3-IRESCre* mutants have coronary artery (CA) defects. Most commonly, we see a single CA arising from the right cusp of a normal aortic valve. Coronary vessels are derived from cells in the proepicardial organ (PEO, a hepatic-derived structure) that invade the tubular heart and become ECs, VSMCs and pericytes of the coronary vasculature and main CAs (Mikawa and Gourdie, 1996). Although NC does not contribute structurally to the CAs (Jiang et al., 2000; Li et al., 2002), CA defects have been described in NC-ablated chicks (Hood and Rosenquist, 1992; Waldo et al., 1994) and in murine mutants of Connexin43 (Li et al., 2002). Cx43 is expressed in both NC and PEO cells; however, the phenotype of Cx43-null mice suggests that the CA defects are due to abnormal migration and/or survival of PEO-derived VSMCs in combination with perturbed interactions between NC and PEO-derived cells in the region of the developing CAs and aortic valve (Li et al., 2002). FGF8 is produced in PA ectoderm adjacent to the PEO; deficiency or ablation of FGF8 in this domain may have similar effects. Further investigation of the entire cardiac vasculature and expression of Cx43 and other intercellular adhesion molecules that participate in CA development, such as α4-integrin or VCAM1 (Kwee et al., 1995; Yang et al., 1996) in *Fgf8* mutants is warranted, in addition to examination of survival, proliferation and differentiation of PEO cells. We have not yet determined if *Fgf8* or our Cre-drivers are expressed in the proepicardial organ; if so, FGF8 autocrine or paracrine actions could play a role in coronary vascular development.

Bicuspid aortic valve (BAV) is a mild form of OFT defect and is the most common human congenital cardiac malformation. Semilunar (aortic and pulmonary) valve formation requires interactions between endocardial and NC-derived mesenchymal cells and myocardium (Ya et al., 1998). NC progeny are present during formation of the aortic valve leaflets at E13.5 and postnatally in the leaflets and tissues adjacent to the CA orifices (Jiang et al., 2000). NC ablation or dysfunction results in severe OFT defects and mild semilunar valve defects, such as BAV. However, existing mouse models of abnormal semilunar valve development result from disruption of endocardially expressed genes (de la Pompa et al., 1998; Lee et al., 2000; Ranger et al., 1998; Ya et al., 1998). BAV in *Fgf8;hoxa3-IRESCre* mutants is attributable to FGF8 ablation in the endoderm since *Fgf8;AP2α*-IRES*Cre* mutants have normal aortic valves. However, the cellular and molecular etiologies of this defect require further investigation in the context of altered FGF8 signaling.

The OFT septum is derived largely from NC, and ablation or dysfunction of NC results in severe OFT defects (Bockman et al., 1989; Conway et al., 1997a; Conway et al., 1997b; Conway et al., 1997c; Epstein et al., 2000; Franz, 1989; Goulding et al., 1993; Jiang et al., 2000; Kirby and Waldo, 1990). Whole-mount TUNEL and analyses of NC apoptosis in the different classes of *Fgf8* mutants presented herein indicate that abnormal NC apoptosis at the 25-27 ss does not cause the severe OFT defects observed in *Fgf8* hypomorphs. Most NC destined for the OFT may have already traversed PAs 3-6 by this somite stage, although OFT septation has not begun. In fact, separation of severe OFT defects (which probably involve some manner of NC dysfunction) from glandular and vascular defects in different classes of *Fgf8* mutants, implies that FGF8 influences on NC are location and time dependent. This raises the exciting possibility that subsets of NC, with distinct structural fates, migrate through the PAs at different times and are supported by distinct domains of FGF8 expression.

Outflow tract formation is not dependent on *Fgf8* expression in the PA epithelia

Our findings indicate that the frequent, severe defects in cardiac OFT alignment, septation and growth seen in *Fgf8* hypomorphs result from altered FGF8 signaling at an earlier stage in the endoderm, or from abnormalities resulting from decreased FGF8 in the primary and/or putative secondary heart field. Because only one out of 33 *Fgf8;hoxa3-IRESCre* mutants had a severe OFT defect and BAV, we hypothesize that onset of *hoxa3-IRESCre* activity in the endoderm (at approximately the 18 ss) may be at a relatively late stage of endoderm function

during OFT development, and that BAV is a manifestation of late endodermal FGF8 deficiency (similar to our hypothesis regarding the glandular defects in these mutants). Expected 'wobble' in this biological system could result in occasional earlier Cre activity in the endoderm and the rare occurrence of more severe OFT defects.

Ablation of FGF8 in early endoderm and cardiac mesoderm (but not PA ectoderm) with a *Tbx1Cre* transgene results in severe OFT defects, but normal development of fourth PAA-derived vessels (J. Epstein, personal communication). Although this experiment confirms the crucial roles of distinct *Fgf8* expression domains in different aspects of pharyngeal and cardiovascular morphogenesis, the question remains whether the crucial source of FGF8 for OFT development is derived from mesoderm or endoderm. Other groups have reported that *Tbx1* is not expressed in precardiac mesoderm (Yamagishi et al., 2003), which would suggest that early endoderm is the requisite source. We are developing early endoderm-specific and precardiac mesoderm Cre drivers to definitively address this question.

We thank Ethan Reichert, Tyler Gasser and Jennetta Hammond for technical assistance; Dr Mario Capecchi and the Capecchi laboratory for helpful discussions and support; Dr Gary Schoenwolf, Dr Kirk Thomas, Dr Lisa Urness, Dr Guy Zimmerman and members of the Li laboratory for critical reading of the manuscript; Karl Lustig, Carol Lenz, Gail Peterson, Sheila Barnett and Julie Tomlin and all vivarium staff for their expertise. B.H. and D.F. are supported by the University of Utah Children's Health Research Center. A.M.M. is supported by the Program in Human Molecular Biology and Genetics, and NIH R01HD044157-01.

References

Abu-Issa, R., Smyth, G., Smoak, I., Yamamura, K. and Meyers, E. N. (2002). Fgf8 is required for pharyngeal arch and cardiovascular development in the mouse. *Development* **129**, 4613-4625.

Alsan, B. H. and Schultheiss, T. M. (2002). Regulation of avian cardiogenesis by Fgf8 signaling. *Development* **129**, 1935-1943.

Auerbach, R. (1960). Morphogenetic interactions in the development of hte mouse thymus gland. *Dev. Biol.* **2**, 271-284.

Bockman, D. E. and Kirby, M. L. (1984). Dependence of thymus development on derivatives of the neural crest. *Science* **223**, 498-500.

Bockman, D. E., Redmond, M. E. and Kirby, M. L. (1989). Alteration of early vascular development after ablation of cranial neural crest. *Anat. Rec.* **225**, 209-217.

Brewer, S., Jiang, X., Donaldson, S., Williams, T. and Sucov, H. M. (2002). Requirement for AP-2alpha in cardiac outflow tract morphogenesis. *Mech. Dev.* **110**, 139-149.

Cleaver, O. and Krieg, P. A. (1999). Molecular mechanisms of vascular development. In *Heart Development* (ed. N. Rosenthal and R. P. Harvey), pp. 221-252. San Diego: Academic Press.

Conway, S. J., Godt, R. E., Hatcher, C. J., Leatherbury, L., Zolotouchnikov, V. V., Brotto, M. A., Copp, A. J., Kirby, M. L. and Creazzo, T. L. (1997a). Neural crest is involved in development of abnormal myocardial function. *J. Mol. Cell. Cardiol.* **29**, 2675-2685.

Conway, S. J., Henderson, D. J. and Copp, A. J. (1997b). Pax3 is required for cardiac neural crest migration in the mouse: evidence from the splotch (Sp2H) mutant. *Development* **124**, 505-514.

Conway, S. J., Henderson, D. J., Kirby, M. L., Anderson, R. H. and Copp, A. J. (1997c). Development of a lethal congenital heart defect in the splotch (Pax3) mutant mouse. *Cardiovasc. Res.* **36**, 163-173.

Crossley, P. H. and Martin, G. R. (1995). The mouse Fgf8 gene encodes a family of polypeptides and is expressed in regions that direct outgrowth and patterning in the developing embryo. *Development* **121**, 439-451.

de la Pompa, J. L., Timmerman, L. A., Takimoto, H., Yoshida, H., Elia, A. J., Samper, E., Potter, J., Wakeham, A., Marengere, L., Langille, B. L. et al. (1998). Role of the NF-ATc transcription factor in morphogenesis of cardiac valves and septum. *Nature* **392**, 182-186.

Dymecki, S. M. (1996). Flp recombinase promotes site-specific recombination in embryonic stem cells and transgenic mice. *Proc. Natl. Acad. Sci. USA* **93**, 6191-6196.

Epstein, J. A. (2001). Developing models of DiGeorge syndrome. *Trends Genet.* **17**, S13-S17.

Epstein, J. A., Li, J., Lang, D., Chen, F., Brown, C. B., Jin, F., Lu, M. M., Thomas, M., Liu, E., Wessels, A. et al. (2000). Migration of cardiac neural crest cells in Splotch embryos. *Development* **127**, 1869-1878.

Frank, D. U., Fotheringham, L. K., Brewer, J. A., Muglia, L. J., Tristani-Firouzi, M., Capecchi, M. R. and Moon, A. M. (2002). An Fgf8 mouse mutant phenocopies human 22q11 deletion syndrome. *Development* **129**, 4591-4603.

Franz, T. (1989). Persistent truncus arteriosus in the Splotch mutant mouse. *Anat. Embryol.* **180**, 457-464.

Garel, S., Huffman, K. J. and Rubenstein, J. L. (2003). Molecular regionalization of the neocortex is disrupted in Fgf8 hypomorphic mutants. *Development* **130**, 1903-1914.

Goulding, M., Sterrer, S., Fleming, J., Balling, R., Nadeau, J., Moore, K. J., Brown, S. D., Steel, K. P. and Gruss, P. (1993). Analysis of the Pax-3 gene in the mouse mutant splotch. *Genomics* **17**, 355-363.

Graham, A. (2001). The development and evolution of the pharyngeal arches. *J. Anat.* **199**, 133-141.

Graham, A. and Smith, A. (2001). Patterning the pharyngeal arches. *BioEssays* **23**, 54-61.

Hood, L. C. and Rosenquist, T. H. (1992). Coronary artery development in the chick: origin and deployment of smooth muscle cells, and the effects of neural crest ablation. *Anat. Rec.* **234**, 291-300.

Jackson, R. J., Howell, M. T. and Kaminski, A. (1990). The novel mechanism of initiation of picornavirus RNA translation. *Trends Biochem Sci.* **15**, 477-483.

Jang, S. K. and Wimmer, E. (1990). Cap-independent translation of encephalomyocarditis virus RNA: structural elements of the internal ribosomal entry site and involvement of a cellular 57-kD RNA-binding protein. *Genes Dev.* **4**, 1560-1572.

Jerome, L. A. and Papaioannou, V. E. (2001). DiGeorge syndrome phenotype in mice mutant for the T-box gene, Tbx1. *Nat. Genet.* **27**, 286-291.

Jiang, X., Rowitch, D. H., Soriano, P., McMahon, A. P. and Sucov, H. M. (2000). Fate of the mammalian cardiac neural crest. *Development* **127**, 1607-1616.

Kirby, M. L. and Waldo, K. L. (1990). Role of neural crest in congenital heart disease. *Circulation* **82**, 332-340.

Kirby, M. L. and Waldo, K. L. (1995). Neural crest and cardiovascular patterning. *Circ. Res.* **77**, 211-215.

Kirby, M. L., Turnage, K. L., 3rd and Hays, B. M. (1985). Characterization of conotruncal malformations following ablation of 'cardiac' neural crest. *Anat. Rec.* **213**, 87-93.

Kirby, M. L., Hunt, P., Wallis, K. and Thorogood, P. (1997). Abnormal patterning of the aortic arch arteries does not evoke cardiac malformations. *Dev. Dyn.* **208**, 34-47.

Kwee, L., Baldwin, H. S., Shen, H. M., Stewart, C. L., Buck, C., Buck, C. A. and Labow, M. A. (1995). Defective development of the embryonic and extraembryonic circulatory systems in vascular cell adhesion molecule (VCAM-1) deficient mice. *Development* **121**, 489-503.

LeDouarin, N. and Jotereau, F. V. (1975). Tracing of cells of the avian thymus through embryonic life in interspecific chimeras. *J. Exp. Med.* **142**.

Lee, T. C., Zhao, Y. D., Courtman, D. W. and Stewart, D. J. (2000). Abnormal aortic valve development in mice lacking endothelial nitric oxide synthase. *Circulation* **101**, 2345-2348.

LeLievre, C. S. and LeDouarin, N. (1975). Mesenchymal derivatives of the neural crest: analysis of chimaeric quail and chick embryos. *J. Embryol. Exp. Morphol.* **34**, 125-154.

Li, J., Chen, F. and Epstein, J. A. (2000). Neural crest expression of Cre recombinase directed by the proximal Pax3 promoter in transgenic mice. *Genesis* **26**, 162-164.

Li, W. E., Waldo, K., Linask, K. L., Chen, T., Wessels, A., Parmacek, M. S., Kirby, M. L. and Lo, C. W. (2002). An essential role for connexin43 gap junctions in mouse coronary artery development. *Development* **129**, 2031-2042.

Lindsay, E. (2001). Chromosomal microdeletions: dissecting del22q11 syndrome. *Nat. Rev. Gen* **2**, 858-868.

Lindsay, E. A., Vitelli, F., Su, H., Morishima, M., Huynh, T., Pramparo, T., Jurecic, V., Ogunrinu, G., Sutherland, H. F., Scambler, P. J. et al.

(2001). Tbx1 haploinsufficiency in the DiGeorge syndrome region causes aortic arch defects in mice. *Nature* **410**, 97-101.

MacArthur, C. A., Lawshe, A., Xu, J., Santos-Ocampo, S., Heikinheimo, M., Chellaiah, A. T. and Ornitz, D. M. (1995). FGF-8 isoforms activate receptor splice forms that are expressed in mesenchymal regions of mouse development. *Development* **121**, 3603-3613.

Manley, N. R. and Capecchi, M. R. (1995). The role of Hoxa-3 in mouse thymus and thyroid development. *Development* **121**, 1989-2003.

Merscher, S., Funke, B., Epstein, J. A., Heyer, J., Puech, A., Lu, M. M., Xavier, R. J., Demay, M. B., Russell, R. G., Factor, S. et al. (2001). TBX1 is responsible for cardiovascular defects in velo-cardio-facial/DiGeorge syndrome. *Cell* **104**, 619-629.

Meyers, E. N. and Martin, G. R. (1999). Differences in left-right axis pathways in mouse and chick: functions of FGF8 and SHH. *Science* **285**, 403-406.

Meyers, E. N., Lewandoski, M. and Martin, G. R. (1998). An Fgf8 mutant allelic series generated by Cre- and Flp-mediated recombination. *Nat. Genet.* **18**, 136-141.

Mikawa, T. and Gourdie, R. G. (1996). Pericardial mesoderm generates a population of coronary smooth muscle cells migrating into the heart along with ingrowth of the epicardial organ. *Dev. Biol.* **174**, 221-232.

Mitchell, P. J., Timmons, P. M., Hebert, J. M., Rigby, P. W. and Tjian, R. (1991). Transcription factor AP-2 is expressed in neural crest cell lineages during mouse embryogenesis. *Genes Dev.* **5**, 105-119.

Moon, A. M., Boulet, A. M. and Capecchi, M. R. (2000). Normal limb development in conditional mutants of Fgf4. *Development* **127**, 989-996.

Moon, A. M. and Capecchi, M. R. (2000). FGF8 is required for outgrowth and patterning of the limbs. *Nat. Genet.* **26**, 455-459.

Ranger, A. M., Grusby, M. J., Hodge, M. R., Gravallese, E. M., de la Brousse, F. C., Hoey, T., Mickanin, C., Baldwin, H. S. and Glimcher, L. H. (1998). The transcription factor NF-ATc is essential for cardiac valve formation. *Nature* **392**, 186-190.

Reifers, F., Walsh, E. C., Leger, S., Stainier, D. Y. and Brand, M. (2000). Induction and differentiation of the zebrafish heart requires fibroblast growth factor 8 (fgf8/acerebellar). *Development* **127**, 225-235.

Sauer, B. and Henderson, N. (1988). Site-specific DNA recombination in mammalian cells by the Cre recombinase of bacteriophage P1. *Proc. Natl. Acad. Sci. USA* **85**, 5166-5170.

Scambler, P. J. (2000). The 22q11 deletion syndromes. *Hum. Mol. Genet.* **9**, 2421-2426.

Schwenk, F., Baron, U. and Rajewsky, K. (1995). A cre-transgenic mouse strain for the ubiquitous deletion of loxP-flanked gene segments including deletion in germ cells. *Nucleic Acids Res.* **23**, 5080-5081.

Soriano, P. (1999). Generalized lacZ expression with the ROSA26 Cre reporter strain. *Nat. Genet.* **21**, 70-71.

Stadler, H. S., Higgins, K. M. and Capecchi, M. R. (2001). Loss of Eph-receptor expression correlates with loss of cell adhesion and chondrogenic capacity in Hoxa13 mutant limbs. *Development* **128**, 4177-4188.

Storm, E. E., Rubenstein, J. L. and Martin, G. R. (2003). Dosage of Fgf8 determines whether cell survival is positively or negatively regulated in the developing forebrain. *Proc. Natl. Acad. Sci. USA* **100**, 1757-1762.

Sun, X., Meyers, E. N., Lewandoski, M. and Martin, G. R. (1999). Targeted disruption of Fgf8 causes failure of cell migration in the gastrulating mouse embryo. *Genes Dev.* **13**, 1834-1846.

Sun, X., Lewandoski, M., Meyers, E. N., Liu, Y. H., Maxson, R. E., Jr and Martin, G. R. (2000). Conditional inactivation of Fgf4 reveals complexity of signalling during limb bud development. *Nat. Genet.* **25**, 83-86.

Trumpp, A., Depew, M. J., Rubenstein, J. L., Bishop, J. M. and Martin, G. R. (1999). Cre-mediated gene inactivation demonstrates that FGF8 is required for cell survival and patterning of the first branchial arch. *Genes Dev* **13**, 3136-3148.

Vitelli, F., Taddei, I., Morishima, M., Meyers, E. N., Lindsay, E. A. and Baldini, A. (2002). A genetic link between Tbx1 and fibroblast growth factor signaling. *Development* **129**, 4605-4611.

Waldo, K. L., Kumiski, D. H. and Kirby, M. L. (1994). Association of the cardiac neural crest with development of the coronary arteries in the chick embryo. *Anat. Rec.* **239**, 315-331.

Ya, J., Schilham, M. W., de Boer, P. A., Moorman, A. F., Clevers, H. and Lamers, W. H. (1998). Sox4-deficiency syndrome in mice is an animal model for common trunk. *Circ. Res.* **83**, 986-994.

Yamagishi, H., Maeda, J., Hu, T., McAnally, J., Conway, S. J., Kume, T., Meyers, E. N., Yamagishi, C. and Srivastava, D. (2003). Tbx1 is regulated by tissue-specific forkhead proteins through a common Sonic hedgehog-responsive enhancer. *Genes Dev.* **17**, 269-281.

Yang, J. T., Rando, T. A., Mohler, W. A., Rayburn, H., Blau, H. M. and Hynes, R. O. (1996). Genetic analysis of alpha 4 integrin functions in the development of mouse skeletal muscle. *J. Cell Biol.* **135**, 829-835.